CONF-850670--11

CONF-850670--11

DE85 010500

SHAPS-2: A Three-Dimensional Computer Program for Linear/Non-linear, Static/Dynamic Analyses of Piping Systems

C. Y. Wang*
Reactor Analysis and Safety Division
Argonne National Laboratory
9700 South Cass Avenue
Argonne, Illinois 60439, U.S.A.

DISCLAIMER

*Member ASME

21p

ABSTRACT

A three-dimensional computer program for linear/non-linear, static/dynamic analyses of reactor-piping systems under various accident loads is described. In the analysis, the hydrodynamic calculation can be performed in the implicit or semi-implicit manner. The structure response can be calculated using either a purely explicit or implicit time-integration scheme. Coupling between the fluid and structure is achieved by utilizing either the implicit-explicit or implicit-implicit link. Thus, a wide range of piping safety problems can be analyzed by the suitable choice of options available in the hydrodynamics and structural analysis.

In this paper, several salient features are presented. Sample problems illustrating the versatility of the program are given. The results are discussed in detail.

INTRODUCTION

Maintaining the structural integrity of the piping system of Liquid Metal Fast Breeder Reactors (LMFBRs) is essential to the safe operation of the reactor and steam supply systems. In the safety analysis various accident loads can be imposed on the piping systems, which may pose threats to the integrity of the piping structure. They are: (1) hydrodynamic loading resulting from pressure-wave propagation due to a hypothetical core-disruptive accident (HCDA) or a sodium-water reactor (SWR); (2) thermal loading generated by hot coolant suddenly entering into the piping system; (3) structural loads due to seismic events; and (4) loads encountered during normal reactor operational transients such as internal pressurization, thermal effects, and creep phenomena. These loads can further be classified into two categories. The first represents dynamic loads resulting from the hydrodynamic pressure-wave propagation or seismic events. The second represents static or quasi-dynamic loads generated by thermal wave propagation, normal operation transient, or creep phenomena. Thus, from a safety analysis point of view development of computer programs capable of performing linear/nonlinear, static/dynamic analysis of piping systems is highly desirable.

Piping loads imposed by internal hydrodynamic forces emanating from a HCDA and a SWR can be the most significant loads to be considered in the safety analysis of LMFBR piping systems. One common feature during such accidents is the propagation and interaction of pressure pulses around a series of elbows and in line components, which can produce substantial loads on a piping system. Note that the pulse itself will be affected by the motion of the piping in that it may be distorted, reduced, or even amplified depending on whether the pipe motion is in or out of phase with the pulse. As a result, an accurate determination of pipe loads requires that the fluid-structure interaction (FSI) for the piping system be considered. Furthermore, in the construction of models to represent realistic accident situations, the analytical methods must be capable of handling problems in three-dimensional space.

Since 1975 substantial research efforts have been devoted to the development of numerical techniques for analyzing pressure-wave transients in reactor piping systems. Piping systems subjected to internal hydrodynamic loads generally are analyzed either by a one-dimensional characteristic method or a two-step approach. The characteristic method partially considers the effect of FSI through a weak coupling scheme via a Joukowski sound-speed modification, but has difficulty in treating large in-line components in which the fluid motion are essentially multi dimensional. The two-step approach, though can treat multi-dimensional fluid motions; however, it quite often leads to over-conservative results since it completely ignores the FSI and calculates the piping response separately from pressure supplied by a rigid-wall hydrodynamic analysis.

To analyze pressure-wave propagation in an LMFBR piping system, a multi-dimensional fluid-structure-interaction method and its associated computer program, called SHAPS [1-3] (Structural Hydrodynamic Analysis of Piping System), has been developed at Argonne National Laboratory. It utilizes a 2-D implicit finite-difference hydrodynamics in conjunction with a 3-D explicit finite-element structural analysis. A 3-D pipe element with eight degrees of freedom is employed to account for the hoop, flexural, axial, and the tor-

sional modes of the piping systems. This method is well suited for analyzing highly nonlinear FSI problems involving high intensity pressure loadings.

Recently, many improvements have been made which has resulted in a second version of the code, SHAPS-2. Specifically, we have introduced several new features, including: (1) a pipe-elbow hydrodynamic model for analyzing the effect of global motion on the pressure-wave propagation, (2) a component hydrodynamic model for treating fluid motion in the vicinity of rigid obstacles and baffle plates, (3) the addition of the implicit time-integration scheme in the structural analysis, which is designed for piping analysis under long-duration loadings.

With these improvements the SHAPS-2 code is now capable of performing linear/nonlinear, static/dynamic analysis of piping systems through proper choice of options in the hydrodynamics and structural analysis. For instance, for the short transient, nonlinear FSI problems, the combination of implicit or semi-implicit hydrodynamic calculation and explicit structural analysis is preferred. For the thermal or seismic problems involving long-duration calculation, implicit hydrodynamics and structural analysis are generally utilized.

HYDRODYNAMICS OF PIPE-ELBOW LOOP

To account for the global motion of the pipe-elbow loop, the governing hydrodynamic equations are written with coordinates fixed to the piping. Let us consider a control volume V bounded by a surface S and moving with arbitrary velocity $\bar{V}^G$. The conservation of mass and momentum of the fluid flowing through V are:

$$\frac{\partial \rho}{\partial t} + (\rho \bar{V}^D)_{i,i} = 0 \tag{1}$$

and

$$\frac{\partial \rho \bar{V}_i}{\partial t} + (\rho \bar{V}_i \bar{V}^D_j)_{,j} + p_{,i} = 0 \tag{2}$$

where

$$\bar{V}^D = \bar{V} - \bar{V}^G$$

is the velocity of the fluid relative to the moving grids. ρ is the density; t is the time; p is the pressure. Note that Eqs. (1-2) are written in standard index notations. These equations indicate that only the convective terms are modified to accommodate the motion of the control volume V.

The governing differential equations can be deducted from Eqs. (1) and (2). Note that the fluid and the finite-difference mesh are moving together in the transverse direction, one can easily see that such a motion is equivalent to a case in which the control volume is fixed in the radial direction, i.e., u^G (the radial velocity component of $\bar{V}^G$) is zero.

Deriving from the moving control volumes shown in Fig. 1 the mass and two momentum equations in terms of the cylindrical coordinates are:

$$\frac{\partial \rho}{\partial t} + \frac{1}{r}\frac{\partial (r\rho u^D)}{\partial r} + \frac{1}{r}\frac{\partial (\rho v^D)}{\partial \theta} = 0 \tag{3}$$

$$\frac{\partial (\rho u)}{\partial t} + \frac{1}{r}\frac{\partial (\rho u^2 r)}{\partial r} + \frac{1}{r}\frac{\partial (\rho u v^D)}{\partial \theta} - \frac{\rho v^2}{r} = -\frac{\partial (p+q')}{\partial r} + \mu \frac{\partial}{\partial \theta}\left[\frac{\partial u}{\partial \theta} - \frac{\partial (rv)}{\partial r}\right] \tag{4}$$

$$\frac{\partial (\rho v)}{\partial t} + \frac{1}{r}\frac{\partial (\rho u v r)}{\partial r} + \frac{1}{r}\frac{\partial (\rho v v^D)}{\partial \theta} + \frac{\partial uv}{r} = -\frac{1}{r}\frac{\partial (p+q')}{\partial \theta} + \mu \frac{\partial}{\partial r}\left[\frac{1}{r}\left[\frac{\partial (rv)}{\partial r} + \frac{\partial u}{\partial \theta}\right]\right] \tag{5}$$

where

$$v^D = v - v^G$$

and

$$q' = -(\lambda + 2\mu)\frac{1}{r}\left[\frac{\partial (ru)}{\partial r} + \frac{1}{r}\frac{\partial v}{\partial \theta}\right] \tag{6}$$

In the above equations λ and μ are the first and second coefficients of viscosity of the fluid, respectively; u and v are the radial and tangential velocity components.

The above governing equations are similar to the standard Eulerian hydrodynamic equations with only one exception, that v^D appears in some of the convective terms, instead of the standard fluid velocity v. Following the difference scheme of the Implicit Continuous-fluid Eulerian (ICE) Method [4,5] which assigns the pressures and densities to the center of the zone and the velocity components to the center of the zone boundary normal to their direction, the differences between the above governing equations and the standard ICE-like equations are reflected only in the source terms $R_{i+1/2,j}$ and $S_{i,j+1/2}$ of the two momentum equations and $G_{i,j}$ of the Poisson equation. Appendix gives complete finite-difference equations for the elbow region.

COMPONENT FLOW

The in-line components of piping system may consist of baffle plates, tube bundle, and ring-shaped region isolated from the main flow. In the analysis the flow in the in-line components is assumed to be two-dimensional, axisymmetric which can be characterized by the radial (r) and axial (z) coordinates. Also, in the basic hydrodynamic technique, rigid obstacles can be introduced in the computer region to model the isolated flow region. The restriction is that each ring-shaped region must occupy at least one full Eulerian cell with its boundaries located on the cell edges [5].

Baffle plates are built into some piping components such as valves and heat exchangers. Except for the movable gates in valves, the function of most interior walls is to produce a certain flow pattern or to support other interior parts like tube bundles. In general, these baffle plates can deform during the course of the pressure-wave propagation. However, deformable baffles would intersect the Eulerian zone boundaries in various ways and thus create many partial or irregular zones which cause difficulties in the Eulerian method. To simplify the analysis, we assume that the orientation of the baffle plate is either parallel to the radial or axial direction. We further

assume that the baffle plate must be placed on the zone boundary with its dimension exactly equal to the width of the Eulerian zone.

Here, a scheme used in Ref. [5] has been adopted to treat the fluid motion in the vicinity of the baffle plates, rigid obstacles, and the isolated flow regions. The approach appropriately adjusts the velocity field in calculating the source terms of the momentum and Poisson equations in accordance with the inviscid fluid boundary conditions. For instance, for the piping component with ring-shaped obstacles as given in Fig. 2, the velocity field is:

$$\begin{aligned} \tilde{u}_{i+(1/2),j+1} &= 0 \\ \tilde{v}_{i+1,j+(1/2)} &= v_{i,j+(1/2)} \\ \tilde{v}_{i+1,j-(1/2)} &= v_{i,j-(1/2)} \\ \tilde{u}_{i+(3/2),j} &= \frac{r_{i+1}(ru)_{i-(1/2),j}}{r_i r_{i+(3/2)}} \end{aligned} \tag{7}$$

In the above equations, the tilde quantities are the dummy values which are different from those computed by the conservation equations.

STRUCTURAL DYNAMICS

The SHAPS code originally uses an explicit time-integration scheme for the structural calculation [6], which is very efficient for highly dynamic problems with short time scales. However, it becomes extremely inefficient for static or quasi-dynamic problems because of its stability-restricted small time steps.

Here, the development of an optional structural module using the implicit time-integration scheme is addressed. This implicit scheme is unconditionally stable and can be used for long-duration problems in the LMFBR piping system. We will describe here the analytical development of the implicit-time-integration scheme.

Stiffness Matrix

As a first step, we shall develop the stiffness matrix of a 3-D pipe element that considers both hoop and flexural stresses, including bending in both planes. Figure 3 shows a typical element of length ℓ. The $\hat{x}$, $\hat{y}$, and $\hat{z}$ coordinates are the co-rotational coordinates associated with the element. The x, y, and z coordinates are the global coordinates. First, we develop a constant element stiffness matrix $[\hat{K}_e]$ so that in the co-rotational coordinate system we have

$$\{f'\} = [\hat{K}_e]\{d'\} \quad \text{or} \quad \{\Delta f'\} = [\hat{K}_e]\{\Delta d'\} \tag{8}$$

using principle of virtue work, one can show that

$$\{f'\} = \left(\int_V B']^T [C'] [B'] \, dV\right)\{d'\} = [\hat{K}_e]\{d'\} \tag{9}$$

where

$$[\hat{K}_e] = \int_V [B']^T [C'] [B'] \, dV \ , \tag{10}$$

is the element stiffness matrix written in the convective coordinate system; [C'] is the material matrix; [B'] relates the displacements to the strains.

By definition, the [B'] matrix has the form

$$[B'] = [\underset{\sim}{B}_1, \underset{\sim}{B}_2] \ , \tag{11}$$

where

$$[B_I] = [B_{IA}, B_{IB}] \tag{12}$$

$$[B_{IA}] = \begin{bmatrix} \frac{(-1)^I}{\ell} & -\hat{y}\psi_{I,xx} & -\hat{z}\psi_{I,xx} & 0 \\ 0 & 0 & 0 & 0 \\ 0 & 0 & 0 & (-1)^I \frac{r}{\ell} \end{bmatrix} \tag{12a}$$

$$[B_{IB}] = \begin{bmatrix} \hat{z}\phi_{I,xx} & -\hat{y}\phi_{I,xx} & -n\psi_{I,xx} & -n\phi_{I,xx} \\ 0 & 0 & \psi_I/r & \phi_I/r \\ 0 & 0 & 0 & r \end{bmatrix} \tag{12b}$$

In Eq. (12) ψ and ϕ are the shape functions [6], r is the radial coordinate, and prime denotes partial differentiation.

Temporal Integration

For the convenience of developing the implicit-integration algorithm, let us rewrite the global equations of motion in the form

$$[M]\{a_{n+1}\} + \{F^{int}(d_{n+1})\} = \{F^{ext}\} \ , \tag{13}$$

where, understandably, [M], {a}, $\{F^{int}\}$, and $\{F^{ext}\}$ denote the global mass matrix, nodal accelerations, nodal internal and external forces, respectively. The subscript n+1 denotes the advanced-time step. Thus, subscript n used subsequently will denote the previous time cycle. Also, it should be mentioned that the internal force $\{F^{int}\}$ is a function of nodal displacements in the advanced-time cycle.

Furthermore, let us assume that

$$\{d_{n+1}^{i+1}\} = \{d_{n+1}^{i}\} + \{\Delta d\} \ , \tag{14}$$

where superscripts i+1 and i denote the advanced and previous iteration, respectively.

The equations of motion can then be integrated in time by an implicit algorithm based on the Newmark-β difference formulas,

$$\{a_{n+1}\} = [\{d_{n+1}\} - \{d_n\} - \Delta t \{v_n\} - (1/2 - \beta) \Delta t^2 \{a_n\}]/\beta\Delta t^2 \tag{15}$$

The nodal accelerations and velocities corresponding to the advanced iteration can be written as

$$\{a_{n+1}^{i+1}\} = [\{d_{n+1}^{i}\} + \{\Delta d\} - \{d_n\} - \Delta t\,\{v_n\} - (1/2 - \beta)\,\Delta t^2\,\{a_n\}]/\beta\Delta t^2 \qquad (16)$$

and

$$\{v_{n+1}^{i+1}\} = \{v_n\} + (1 - \gamma)\,\Delta t\,\{a_n\} + \gamma\Delta t\,\{a_{n+1}^{i+1}\} \qquad (17)$$

In Eqs. (15-17), β and γ are the integration constants. Based on the method of linearization, the nodal internal force at the advanced-time iteration can be expressed as a function of previous iteration values, or

$$\{F^{int}(d_{n+1}^{i+1})\} \simeq \{F^{int}(d_{n+1}^{i})\} + [K(d_{n+1}^{i})]\,\{\Delta d\} + \ldots . \qquad (18)$$

Substituting Eqs. (16) and (18) into Eq. (13) yields, after some rearranging, a set of linear algebraic equations in the matrix form

$$([M] + \beta\Delta t^2\,[K])\{\Delta d\} = \beta\Delta t^2\,[\{F^{ext}\} - \{F^{int}(d_{n+1}^{i})\}] - [M]\left[\{d_{n+1}^{i}\} - \{d_n\} - \Delta t\{v_n\} - (1/2 - \beta)\Delta t^2\{a_n\}\right] \qquad (19)$$

This equation is compacted by defining the coefficient of $\{\Delta d\}$ as $[K^{eff}]$ and the right-hand side as $\{F^{eff}\}$, thus, we have

$$[K^{eff}]\{\Delta d\} = \{F^{eff}\} \qquad (20)$$

The computational procedure for each time step is described here. The iteration begins with the predicting phase in which the new displacement field, associated with the eight degrees of freedom per node, is approximately computed, based on the previous cycle values in conjunction with the conventional Newmark-Beta formula. This displacement field is utilized to estimate the nodal internal forces. The incremental displacement is solved by the equations of equilibrium expressed by the global stiffness matrix given in Eq. (20). Because of the approximations made in arriving at Eq. (20), the predicted structural motion will not, in general, satisfy the dynamic equilibrium shown in Eq. (13). Under this condition, the incremental displacement is then utilized as a corrector to recompute the displacement, acceleration, and velocity fields, as well as the nodal internal force. The procedure is repeated until convergence is attained.

FLUID-STRUCTURE INTERACTION

The treatment of fluid-structure interaction (FSI) depends on the time-integration scheme used in the hydrodynamic and structural calculations. In the past, the hydrodynamic equations were integrated implicitly, while the structural equations were integrated explicitly and an implicit-explicit (I-E) coupling was utilized. Since, in general, the hydrodynamic time step is much larger than the stability-governed structural time step, several structural subcycles must be performed to match one hydrodynamic calculation. This I-E coupling via structural subcycling could become time consuming for problems involving slowly varying pressures where large hydrodynamic time steps can be utilized. Following the development of the implicit structural module, we have introduced an option which uses implicit-implicit (I-I) coupling in the FSI analysis, with both hydrodynamic and structural equations integrated implicitly. This avoids the structural subcycling and yet maintains the numerical stability.

OTHER IMPROVEMENTS

As discussed at SMiRT-6 in Paris [1], the SHAPS code utilizes a thermoviscoplastic constitutive equation to calculate the thermal stress field. This equation, though, is general but is slow for temperature-independent problems due to additional treatment specifically formulated for thermal effects. Recently, a fast-running, non-linear, purely elastic-plastic constitutive model has been incorporated into SHAPS to treat temperature-independent problems. The governing equations are integrated with a tangent predictor radial return algorithm. Moreover, improvement of efficiency has been made in evaluating stress at various Gaussian stations, which has resulted in a 30-50% reduction of CPU time in many test calculations.

For the analysis of problems involving thermal shock, the existing SHAPS code has the capability of generating fluid temperatures for the straight pipes. Also, an elbow thermal model has recently been developed. A system energy equation, written in terms of the tangential θ coordinate, is utilized to calculate the coolant temperatures inside the elbow region due mainly to the fluid convection. Such an analysis enables the thermal transient analysis of a pipe-elbow loop to be adequately performed.

SAMPLE PROBLEMS

Because of space limitations, only three sample problems are presented here. For additional problems illustrating analyses of three-dimensional piping FSI, seismic excitation, as well as structural response under long-duration load, the reader may refer to a paper presented elsewhere [7].

Experimental Validation

Test FP-E-103 of a single-elbow piping system is one of the simple elastic-plastic piping experiments performed by SRI International [8] for verifying the piping analysis programs. This test is analyzed with the SHAPS-2 code. The purposes are: (1) to validate the hydrodynamic model for treating the global motion of the pipe-elbow loop; (2) to verify the thermoviscoplastic constitutive law for treating the elastic-plastic response of the piping system; and (3) to estimate the pressure attenuation along the elbow.

The experimental setup of Test FP-E-103 is shown in Fig. 4, where a specially designed and calibrated pulse gun is directly flanged to a thick-walled stain-

less pipe 304.8 cm (10 ft) long. The pressure history recorded at gauge P1 was used as input to the SHAPS model. A calculation was performed with a uniform axial zone size of 5.08 cm (2 in), and the elbow region was divided into three tangential zones.

Near the elbow, the pressure histories for transducers P8-P10, located upstream from the elbow, and P14-P16, downstream from the elbow, are compared with the experimental results in Figs. 5 and 6. The agreement between the calculated and measured results is quite good. Because of the global elbow motion, a drop of peak pressure is noticed as the pressure wave travels from upstream to downstream.

To study the effect of global elbow motion, another calculation was performed with SHAPS-2, which ignores the flexural motion of the elbow and treats the elbow as a structure rigidly fixed in space. The results show no drop of peak pressure along the elbow. In other words, the calculated peak pressure at P8-P10 upstream is about the same as that observed at P14-P16 downstream. Therefore, it can be concluded that the calculated pressure attenuation is due to the flexural motion of the elbow in response to the internally propagating pulse.

The good agreement achieved in this study demonstrates the degree of accuracy of SHAPS code capabilities in treating elastic-plastic material and global elbow motion.

Fluid-Structure-Interaction Analysis

A test problem of a straight pipe was used to check the performance of the newly introduced implicit-implicit (I-I) hydrodynamic-structural coupling. A 20-axial zone representation of a straight pipe with inside radius 21.43 cm and length 609.6 cm is utilized as the numerical model, shown in Fig. 7. A non-reflecting boundary is assumed at the junction after the pipe, while a 5-MPa square pulse of 2-ms duration is applied to the junction before the pipe. The thickness of the pipe was 1.428 cm. The yield stress is 6.30×10^9 MPa.

The pressure histories at the non-reflecting junction [zone (2,21)] are shown in Fig. 8. In this figure, the solid lines represent the results of the I-I analysis, while the dashed lines indicate the solutions of I-E calculation. It can be seen that the pressure pulse propagates along the pipe with little change in its shape or its magnitude. Figures 9 and 10 further depict the circumferential strain and stress at node 10 (see Fig. 7 for its location). Results of pressure, strain, and stress histories revealed the close similarity of solutions obtained from the I-I and I-E couplings.

Response of a Three-Dimensional Pipe-Elbow Loop

To test the performance of the implicit structural module, a sample problem which couples different modes of deformation is presented. This pipe system consists of three pipes connected through two 90° elbows as shown in Fig. 11. All pipes and elbows have the same cross-section dimensions with inside radius and wall thickness equal to 3.81 and 0.33 cm, respectively. Both ends of the system are assumed fixed in space. Each elbow has a radius of curvature of 16.2 cm and is represented by five pipe elements.

A point load parallel to the global X-axis is applied at the midpoint of the second pipe as given in Fig. 11. The load is increased linearly from zero to 2000 N in 50 μs and then held constant. The problem was run previously using the explicit time integration scheme [6], and the solutions have been compared with those obtained from the two well-known programs, SAP-IV and WHAMSE [9,10]. Referring to Fig. 11, one can see that pipe 1 is subject to axial and bending loadings, pipe 2 is subject to bending loading, and pipe 3 is subject to bending and torsional loadings.

Static analysis. Static analysis cannot be performed with the explicit structural module. However, it can be obtained easily using the implicit structural module by suppressing the inertia effect. The static analysis provides a permanent, time-independent solution for the pipe-elbow loop. Figure 12 plots the piping configuration with an enlarged scale, using a magnification factor of 50 for easier observation.

Dynamic analysis and its verification. As mentioned before, the explicit calculation has been compared with those of the SAP-IV and WHAMS programs. Thus, its solutions are quite reliable and can be used to verify the implicit solutions. Here, we present the solutions the explicit and implicit time integration, respectively. Note that the explicit calculation consists of 10,000 computational cycles with a small time step of 2.5 μs governed by the stability analysis. On the other hand, the implicit calculation uses a medium time step of 50 μs, which is twenty times larger than the explicit time step.

Excellent agreement between the implicit and explicit solutions was obtained at all locations. One example of such comparisons is shown in Fig. 13 in which the solid line represents the implicit solution and the dashed line represents the explicit solution. It shows the Z-rotation history at node 47 of elbow 2, which represents the twisting rotation at that node.

Effect of time step and computational efficiency. To study the effect of time step on the solution accuracy, we compare the results of three implicit calculations -- Cases A, B, and C -- which use time steps equivalent to 20, 50, and 100 times the explicit time step (run 2), respectively. Again, good agreement among the three solutions was obtained. For illustration, Fig. 14 gives results regarding X-displacement at node 20. It can be seen that the effect of the time step on the implicit solution is extremely small.

ACKNOWLEDGMENTS

The author wishes to thank Drs. T. B. Belytschko and W. K. Liu for many helpful discussions regarding the implicit structural analysis. This work was performed in the Engineering Mechanics Program of the Reactor Analysis and Safety Division of Argonne National Laboratory under the auspices of the U.S. Department of Energy.

REFERENCES

[1] WANG, C. Y., A-MONEIM, M. T., BELYTSCHKO, T. B. "Integrated Analysis of Piping Systems," Trans. 6th Int. Conf. on Structural Mechanics in Reactor Technology, Paper E 6/1, Paris, France (August 1981).

[2] WANG, C. Y., "A Three-Dimensional Method for Integrated Transient Analysis of Reactor-Piping Systems," Nuclear Engineering and Design, Vol. 68, No. 2, pp. 175-184 (March 1982).

[3] WANG, C. Y., "Theory and Application of a Three-Dimensional Code SHAPS to Complex Piping Systems," Advances in Fluid-Structure Interaction, 4th Int. Congress on Pressure Vessel Piping Technology, ASME PVP-75, Book No. H00261, pp. 139-157, Portland, OR (June 1983).

[4] HARLOW, F. H., AMSDEN, A. A., "A Numerical Fluid Dynamics Calculation Method for All Flow Speeds," J. Comp. Phys., Vol. 8, p. 197 (October 1971).

[5] WANG, C. Y., "Analysis of Nonlinear Fluid-Structure Interaction Transient in Fast Reactors," ANL-78-103, Base Technology (November 1978).

[6] A-MONEIM, M. T., CHANG, Y. W., BELYTSCHKO, T. B., "Three-Dimensional Response of Piping Systems to Internally Propagating Pressure Pulses," Trans. 5th Int. Conf. on Structural Mechanics in Reactor Technology, Paper E 3/3, Berlin, Germany (August 1979).

[7] ZEUCH, W. R., WANG, C. Y., "Analysis of Pressure Wave Transients and Seismic Response in LMFBR Piping Systems Using the SHAPS Code," Trans. 8th Int. Conf. on Structural Mechanics in Reactor Technology, Paper E 6/3, Brussels, Belgium (August 1985).

[8] CAGLIOSTRO, D. J., ROMANDER, C. M., "Experiments on the Response of Flexible Piping Systems to Internal Puressure Pulses," SRI Fourth Interim Report on Project PVP-1960, SRI International, Menlo Park, CA (April 1976).

[9] BATHE, K. J., et al., "SAP-IV: A Structural Analysis Program for Static and Dynamic Response of Linear Systems," EERC 73-11, University of California (June 1973).

[10] BELYTSCHKO, T. B., SHWER, L., KLEIN, J. T., "Large Displacement, Transient Analysis of Space Frames," Int. J. of Numerical Methods in Engineering, Vol. 11, p. 65 (1977).

APPENDIX

The finite-difference forms of the radial- and tangential-momentum equations and the governing Poisson equation are:

$$\frac{(\rho u)^{n+1}_{i+(1/2),j} - (\rho u)^{n}_{i+(1/2),j}}{\delta t} = \frac{\phi}{\delta r}\left(p^{n+1}_{i,j} - p^{n+1}_{i+1,j}\right) + \frac{1-\phi}{\delta r}\left(p^{n}_{i,j} - p^{n}_{i+1,j}\right) + CR_{i+(1/2),j} \qquad (A1)$$

and

$$\frac{(\rho v)^{n+1}_{i,j+(1/2)} - (\rho v)^{n}_{i,j+(1/2),j}}{\delta t} = \frac{\phi}{r_i \delta\theta}\left(p^{n+1}_{i,j} - p^{n+1}_{i,j+1}\right) + \frac{1-\phi}{r_i \delta\theta}\left(p^{n}_{i,j} - p^{n}_{i,j+1}\right) + CS_{i,j+(1/2)} \qquad (A2)$$

$$p^{n+1}_{i,j}\left[\frac{1}{c^{n}_{i,j}} + 2\phi\beta\delta t^2\left(\frac{1}{\delta r^2} + \frac{1}{r_i^2 \delta\theta^2}\right)\right] = CG_{i,j} + \phi\beta\delta t^2\left[\frac{r_{i+(1/2)}p^{n+1}_{i+1,j} + r_{i-(1/2)}p^{n+1}_{i-1,j}}{r_i \delta r^2} + \frac{p^{n+1}_{i,j+1} + p^{n+1}_{i,j-1}}{r_i^2 \delta\theta^2}\right] \qquad (A3)$$

In Eqs. (A1-A3), ϕ and β are the weighting constants used in the momentum and mass equations, respectively. These constants, with values between 0.0 and 1.0, represent the relative level of time centering of pressure gradient and mass convection respectively. As an example, for $\phi = 1.0$, the pressure gradient terms is expressed at the advanced time and the technique is purely implicit. For $\phi = 0.5$, the pressure gradient term is time-centered and the technique is semi-implicit-explicit. The source term for the radial-momentum equation in the elbow region is:

$$CR_{i+(1/2),j} = \frac{u_{i+(1/2),j}}{r_{i+(1/2)}\delta r}\left[r_i \rho_{i,j} u_{i-(1/2),j} - r_{i+1}\rho_{i+1,j}u_{i+(3/2),j}\right] + \frac{1}{r_{i+(1/2)}\delta\theta}\left[(\rho uv^D)_{i+(1/2),j-(1/2)} - (\rho uv^D)_{i+(1/2),j+(1/2)}\right] + \frac{1}{r_{i+(1/2)}}\left[\rho_{i+(1/2),j} v_{i+(1/2),j-(1/2)} v_{i+(1/2),j+(1/2)}\right] + \frac{1}{\delta r}\left(q'_{i,j} - q'_{i+1,j}\right) + \frac{\mu}{r^2_{i+(1/2)}\delta\theta}\left\{\frac{u_{i+(1/2),j+1} + 2u_{i+(1/2),j} + u_{i+(1/2),j-1}}{\delta\theta} + \frac{r_i\left[v_{i,j+(1/2)} - v_{i,j-(1/2)}\right]}{\delta r} - \frac{r_{i+1}\left[v_{i+1,j+(1/2)} - v_{i+1,j-(1/2)}\right]}{\delta r}\right\} . \qquad (A4)$$

The source term for the tangential-momentum equation in the elbow region is:

$$CS_{i,j+(1/2)} = \frac{1}{r_i \delta r}$$

$$\left[r_{i-(1/2)} (\rho uv)_{i-(1/2),j+(1/2)} \right.$$

$$\left. - r_{i+(1/2)} (\rho uv)_{i+(1/2),j+(1/2)} \right]$$

$$+ \frac{v_{i,j+(1/2)}}{r_i \delta\theta} \left[\rho_{i,j} v_{i,j-(1/2)} \right.$$

$$\left. - \rho_{i,j+1} v_{i,j+(3/2)} \right]$$

$$- \frac{(\rho uv)_{i,j+(1/2)}}{r_i} + \frac{1}{r_i \delta\theta} (q'_{i,j} - q'_{i,j+1})$$

$$+ \frac{1}{r_i \delta\theta} \left[(\rho u v^G)_{i,j+1} - (\rho v v^G)_{i,j} \right]$$

$$+ \frac{\mu}{\delta r^2} \left[\frac{r_{i+1} v_{i+1,j+(1/2)} - r_i v_{i,j+(1/2)}}{r_{i+(1/2)}} \right.$$

$$\left. + \frac{r_{i-1} v_{i-1,j+(1/2)} - r_i v_{i,j+(1/2)}}{r_{i-(1/2)}} \right]$$

$$+ \frac{\mu}{\delta r \delta\theta} \left[\frac{u_{i+(1/2),j} - u_{i+(1/2),j+1}}{r_{i+(1/2)}} \right.$$

$$\left. + \frac{u_{i+(1/2),j+1} - u_{i-(1/2),j}}{r_{i-(1/2)}} \right] \qquad (A5)$$

The source term for the Poisson equation in the elbow region is:

$$CG_{i,j} = \frac{p^n_{i,j}}{c^n_{i,j}} + \frac{\beta(1-\phi) r_{i+(1/2)} \delta t^2}{r_i \delta r^2} (p^n_{i+1,j} - p_{i,j})$$

$$- \frac{\beta(1-\phi) r_{i-(1/2)} \delta t^2}{r_i \delta r^2} (p^n_{i,j} - p^n_{i-1,j})$$

$$+ \frac{\beta \delta t^2}{r_i \delta r} \left[r_{i-(1/2)} CR_{i-(1/2),j} - r_{i+(1/2)} \right.$$

$$\left. CR_{i+(1/2),j} \right] + \frac{\delta t}{r_i \delta r} \left[r_{i-(1/2)} (\rho u)^n_{i-(1/2),j} \right.$$

$$\left. - r_{i+(1/2)} (\rho u)^n_{i+(1/2),j} \right] + \frac{\beta(1-\phi)\delta t^2}{r_i^2 \delta\theta^2}$$

$$(p^n_{i,j+1} - p_{i,j}) - \frac{\beta(1-\phi)\delta t^2}{r_i^2 \delta\theta^2}$$

$$(p^n_{i,j} - p^n_{i,j-1}) + \frac{\beta \delta t^2}{r_i \delta\theta} \left[CS_{i,j-(1/2)} \right.$$

$$\left. - CS_{i,j+(1/2)} \right] + \frac{\delta t}{r_i \delta\theta} \left[(\rho v)^n_{i,j-(1/2)} \right.$$

$$\left. - (\rho v)^n_{i,j+(1/2)} \right] + B \delta t \qquad (A6)$$

where

$$v^D = v - v^G \qquad (A7)$$

$$q' = -(\lambda + 2\mu) \frac{1}{r} \frac{\partial (ru)}{\partial r} + \frac{1}{r} \frac{\partial v}{\partial \theta} \qquad (A8)$$

and

$$B = \frac{1}{r_i \delta\theta} (\rho v^G)^n_{i,j+1/2} - (\rho v^G)^n_{i,j-(1/2)} \qquad (A9)$$

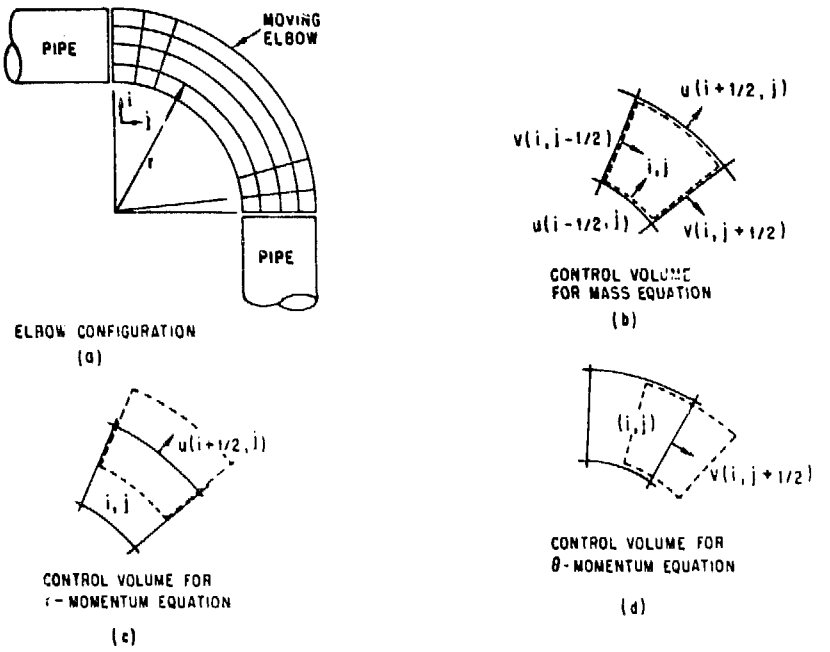

Fig. 1. Elbow Configuration and Control Volumes for Derivation of Hydrodynamic Equations

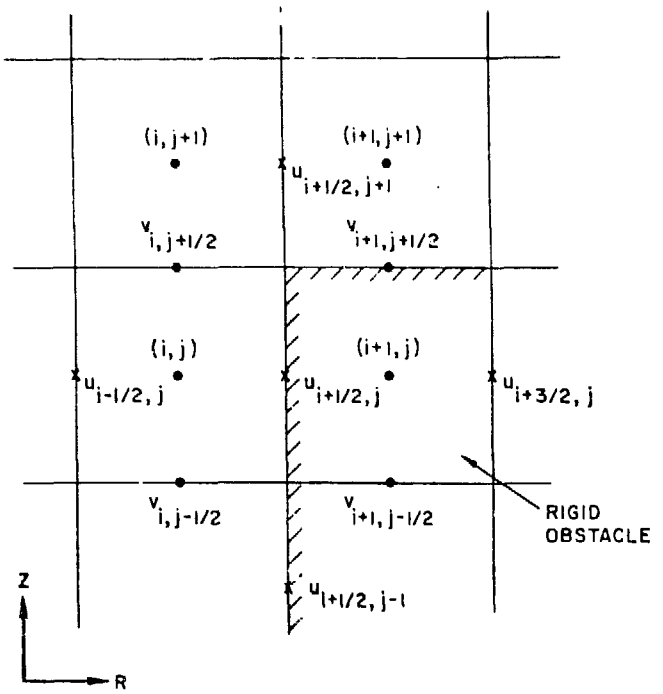

Fig. 2. Velocity Arrangement Near the Ring-Shaped Obstacle Region

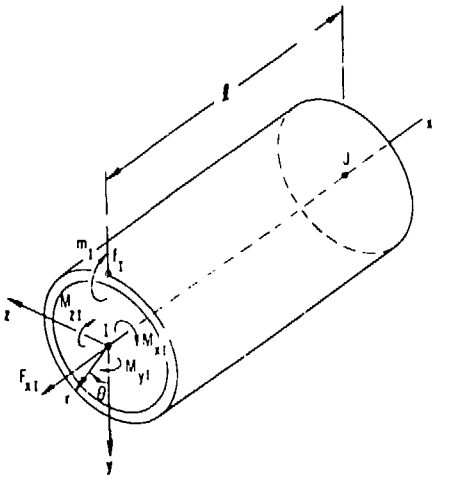

Fig. 3. Generic Pipe Element

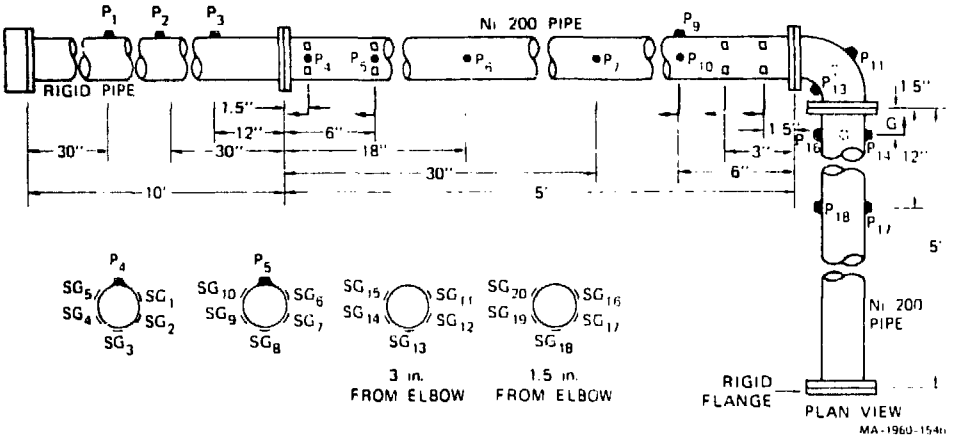

Fig. 4. Layout of the SRI Pipe-Elbow Experiment

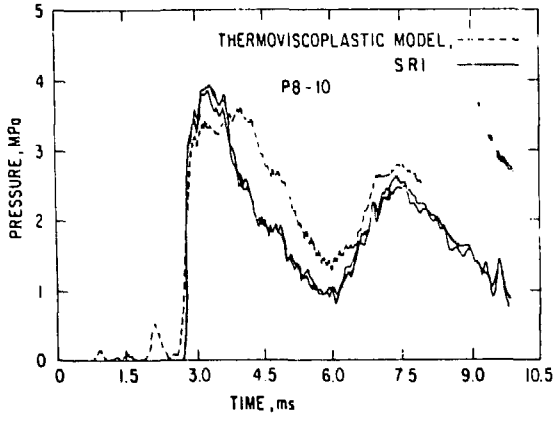

Fig. 5. Pressure Histories of P8-P10 of First Flexible Pipe

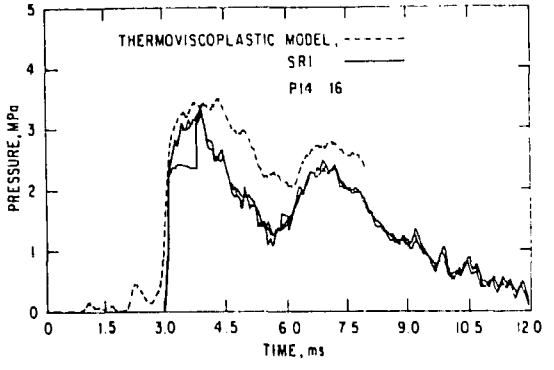

Fig. 6. Pressure Histories at P14-P16 of Second Flexible Pipe

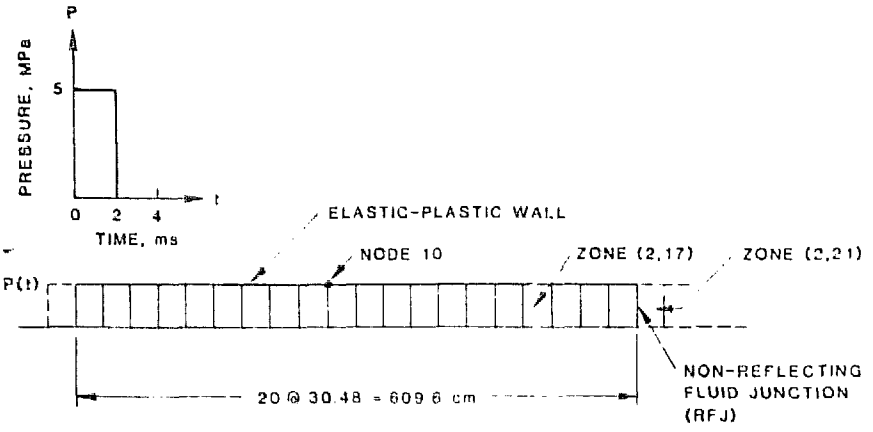

Fig. 7. Configuration of Straight Pipe Used in the SHAPS Analysis

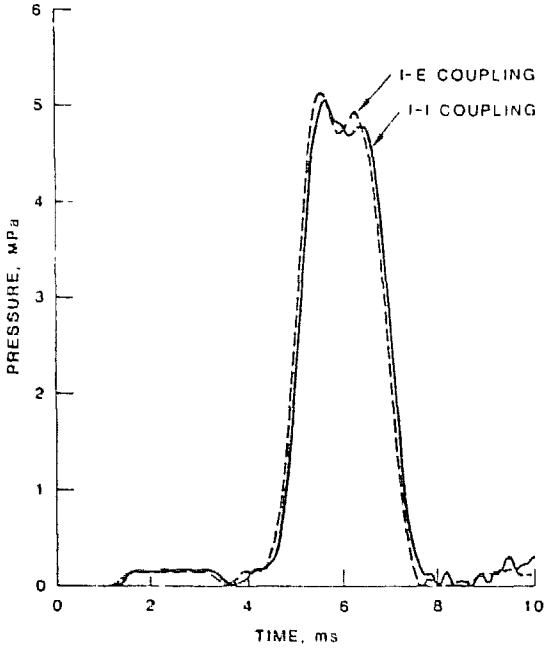

Fig. 8. Pressure Histories at Non-Reflecting Fluid Junction, Zone (2,21)

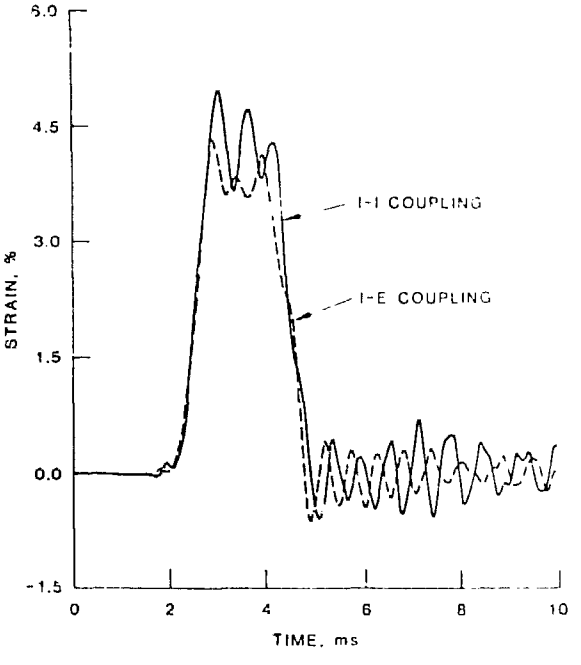

Fig. 9. Time Histories of the Circumferential Strain at Structural Node 10

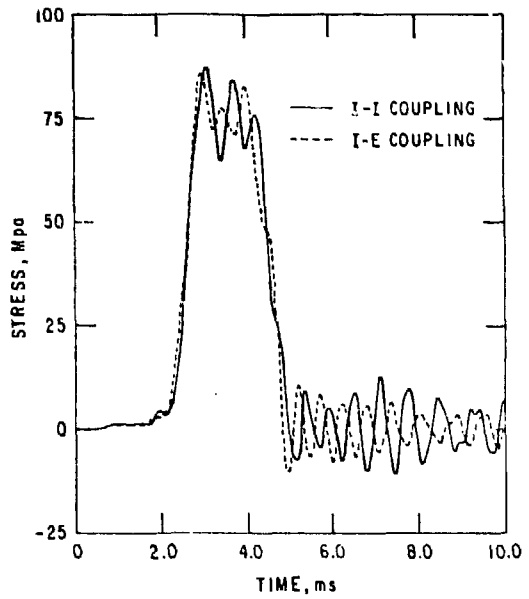

Fig. 10. Time Histories of the Circumferential Stress at Structural Node 10

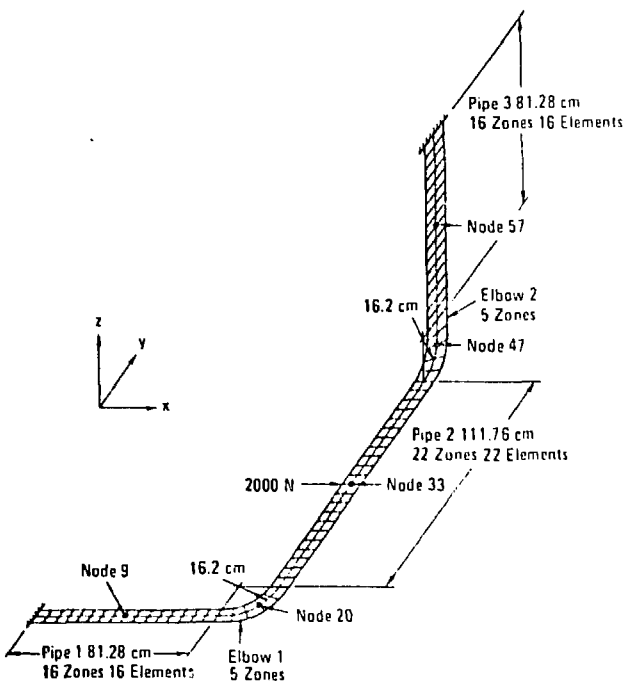

Fig. 11. Model of the Three-Dimensional Piping System

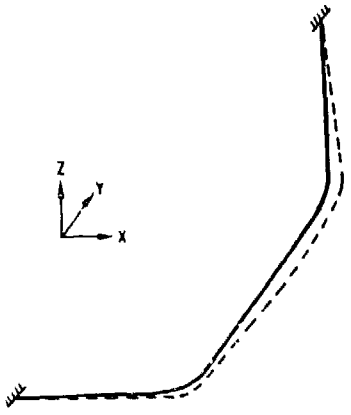

Fig. 12. Piping Configuration Obtained from the Implicit Static Analysis (Multiplication factor = 50)

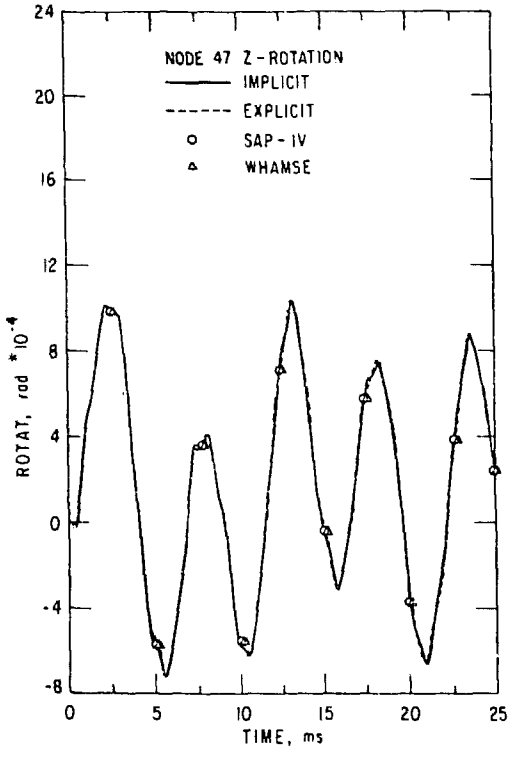

Fig. 13. The Z-Rotation Time History at Node 47 of Elbow 2

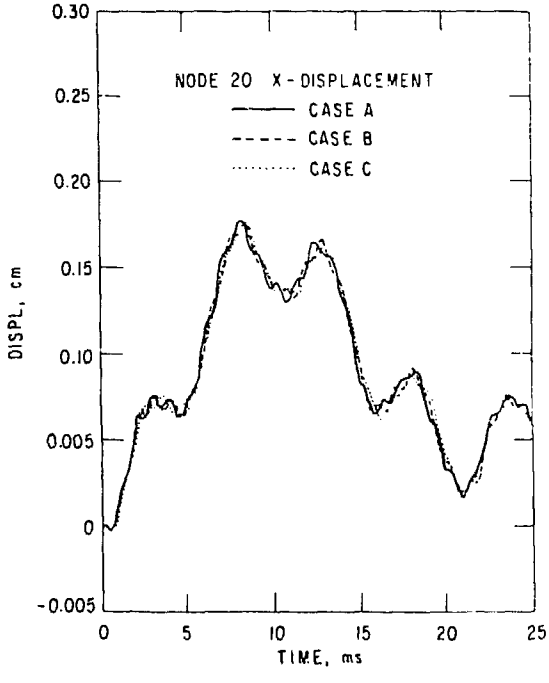

Fig. 14. Comparison of X-Displacement Time Histories at Node 20 of Elbow 1 for Various Implicit Calculations